Neuropixels Opto: Combining high-resolution electrophysiology and optogenetics

Anna Lakunina[1]*, Karolina Z Socha[2]*, Alexander Ladd[3], Anna J Bowen[3], Susu Chen[4], Jennifer Colonell[4,5], Anjal Doshi[1], Bill Karsh[4,5], Michael Krumin[2], Pavel Kulik[1], Anna Li[3], Pieter Neutens[6], John O'Callaghan[6], Meghan Olsen[1], Jan Putzeys[6], Harrie AC Tilmans[6], Zhiwen Ye[3], Marleen Welkenhuysen[6], Michael Häusser[7], Christof Koch[8], Jonathan T. Ting[3,9], Neuropixels Opto Consortium, Barun Dutta[6], Timothy D Harris[4,5], Nicholas A Steinmetz[3], Karel Svoboda[1,4], Joshua H Siegle[1†], Matteo Carandini[2†]

High-resolution extracellular electrophysiology is the gold standard for recording spikes from distributed neural populations, and is especially powerful when combined with optogenetics for manipulation of specific cell types with high temporal resolution. We integrated these approaches into prototype Neuropixels Opto probes, which combine electronic and photonic circuits. These devices pack 960 electrical recording sites and two sets of 14 light emitters onto a 1 cm shank, allowing spatially addressable optogenetic stimulation with blue and red light. In mouse cortex, Neuropixels Opto probes delivered high-quality recordings together with spatially addressable optogenetics, differentially activating or silencing neurons at distinct cortical depths. In mouse striatum and other deep structures, Neuropixels Opto probes delivered efficient optotagging, facilitating the identification of two cell types in parallel. Neuropixels Opto probes represent an unprecedented tool for recording, identifying, and manipulating neuronal populations.

Introduction

Understanding brain function requires recording from myriad neurons, identifying them, and manipulating their activity. For large-scale recordings, an ideal method is extracellular electrophysiology via high-density electrodes such as Neuropixels probes[1,2]. For neuron identification[3-5] and manipulation[6-10], in turn, the best method is optogenetics.

Electrophysiology and optogenetics are particularly powerful when paired with each other[11-13]. By combining them, one can test causality by activating or inactivating specific neuronal populations while recording the effects on neural activity[7,14-17]. One can also identify whether the recorded neurons belong to a genetic class of interest, by inducing this class to express an opsin and stimulating it with light for 'optotagging[3-5]'. Optotagging is critical for connecting the wealth of knowledge about the gene expression, morphology, and connectivity of different cell classes to their function[18].

[1]Allen Institute for Neural Dynamics, Seattle, WA, USA. [2]UCL Institute of Ophthalmology, University College London, London, UK. [3]Department of Neurobiology and Biophysics, University of Washington, Seattle, WA, USA. [4]Janelia Research Campus, Howard Hughes Medical Institute, Ashburn, VA, USA. [5]Department of Biomedical Engineering, Johns Hopkins University, Baltimore, MD, USA. [6]IMEC, Leuven, Belgium. [7]Wolfson Institute for Biomedical Research, University College London, London, UK. [8]Allen Institute MindScope Program, Seattle, WA, USA. [9]Allen Institute for Brain Science, Seattle, WA, USA. *Equal contributors. †Co-senior authors

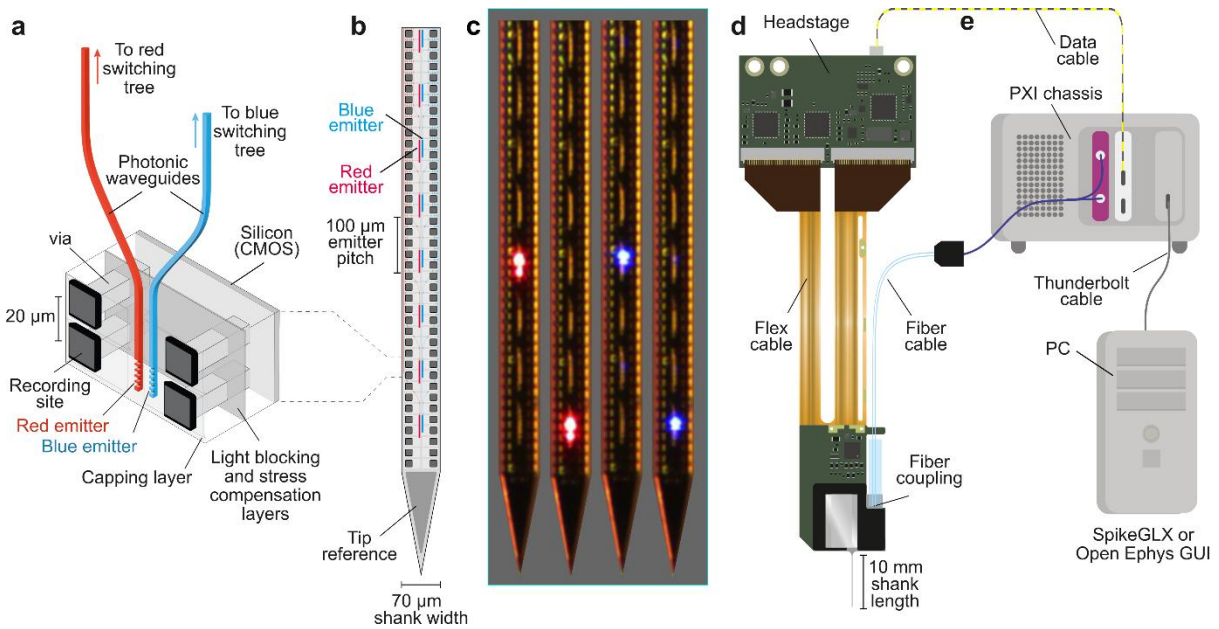

Figure 1 – Design of the prototype Neuropixels Opto probe. **a**, Cross-section of the Neuropixels Opto shank, showing the titanium nitride (TiN) recording sites (connected with a "via" to the silicon CMOS layer) and the silicon nitride (SiN) photonic waveguides ending in the emitters (grating couplers). **b**, Layout of recording sites and dual color emitters. **c**, Photos of a probe shank across four time points, with two red and two blue emitters delivering light in succession. **d**, Device package. e, Neuropixels Opto system architecture, with PXI modules for data acquisition (white) and light delivery (*purple*).

Optogenetics, however, depends critically on delivering light with sufficient intensity and spatial resolution, potentially deep in the brain. This is difficult in brain tissue, which scatters and absorbs light[19]. It commonly requires inserting additional devices for light delivery, such as optical fibers[20-22], waveguides[23], or microLED arrays[24-28]. These approaches, however, limit spatial resolution or light intensity, are invasive, and require a separate device for recording.

There is thus great interest in combining recording and light emission into a single 'optrode', but existing solutions have few recording sites or limited light intensity. Early optrodes integrated electrodes with optical fibers[29-33], yielding few emitters. More emitters were enabled by microLEDs[27,34-38]. However, miniaturized microLEDs have low efficiency (1-3%) so even at moderate light they increase brain temperature[39,40] by 0.5–1.5 °C (Refs. [24,27]). They thus deliver only low light intensities or duty ratios[41].

To resolve these limitations, we combined Neuropixels recording technology with on-chip photonic waveguides that route high-intensity light down the shank of the probe. Light is generated outside the brain and routed by on-chip photonic waveguides[42-46]. This enables dual color illumination across a 1.4 mm span in parallel to voltage readout from close to a thousand selectable recording sites per shank with on-board amplification and digitization[1,2]. The resulting prototype device, called Neuropixels Opto, delivers unprecedented integration of high-resolution electrophysiology and optogenetics.

Results

Neuropixels Opto integrates electronics and photonics to simultaneously record signals from 384 out of 960 recording sites and emit light from two sets of 14 emitters. The two sets of light emitters allow dual color optogenetics with blue and red light, making it possible to manipulate or optotag two genetically defined neural populations in parallel. For the red light, we chose a

wavelength of 638 nm to excite highly effective red-sensitive opsins such as Chrimson[47] and ChRmine[48]. This wavelength avoids the peak of blood absorption[49] around 540 nm and thus enhances the penetration of light into tissue. For the blue light, we set the wavelength to 450 nm (rather than the more common 473 nm) to activate Channelrhodopsin-2 (ChR2[50]) and its variants efficiently, while minimizing the activation of the red-sensitive opsins.

Probe design

The red and blue light is routed to programmable emitters via photonic waveguides (**Figure 1a**). The routing is provided by an integrated silicon nitride (SiN) photonics layer that lies on top of the CMOS platform designed for Neuropixels 1.0 probes[1] (a 130-nm silicon-on-insulator CMOS Al process with 6 metal layers). The waveguides are fabricated in 150 nm thick SiN and are routed to the distal end of the shank. To couple out the light from the waveguides to the emitters and distribute it perpendicular to the probe, we used higher order, apodized Bragg grating couplers[51-54] designed to spread the light over multiple diffraction peaks.

This design posed two challenges. First, the addition of photonics can cause the probe shank to bend. We addressed this challenge by depositing a SiN compensation layer and a SiN capping layer (**Figure 1a**), reducing tip deflection to < 200 μm. Second, scattered light from the photonic waveguides can interact with the CMOS circuitry, increasing noise levels or introducing recording artifacts. To prevent light from reaching the CMOS, we added a TiN/Al-based light blocking layer (**Figure 1a**), keeping it as thin as possible to minimize shank bending and thickness. The emitters (16-25 μm^2) are arranged in a 14x2 layout with 100 μm spacing on the center axis of the shank, starting 100 μm from the first recording site (**Figure 1b,c**). The probe can thus emit light over 1.4 mm from the shank's tip. The recording site array has a similar density to Neuropixels 1.0 (Ref. [1]), with 960 titanium nitride (TiN) 12x12 μm^2 recording sites, but the sites are arrayed in two vertical columns (spaced 20 μm vertically and 48 μm horizontally) rather than a staggered 'checkerboard' layout. The shank is 10 mm long, 70 μm wide, and 33 μm thick. Signals from each recording site are split into 'action potential' (AP, 0.3–10 kHz) and 'local field potential' (LFP, <1 kHz) bands, which are digitized at 30 kHz and 2.5 kHz.

The light is generated by two fiber-coupled lasers at 450 and 638 nm, connected to the probe via grating couplers, and routed to the emitters by two photonic switching trees. There are 8 grating couplers: two to couple the light from the two fibers, and the others for active alignment of the fiber block and for measuring coupling losses. The light of each color is routed to the desired emitters via a programmable photonic binary switching tree (**Supplementary Figure S1**). With 4 levels, the tree can specify 2^4=16 outputs and thus address the 14 emitters. The switches are thermo-optic: Mach-Zehnder interferometers with thermal phase shifters based on the thermo-optic effect[55]. After calibration, they are the optical equivalent of a toggle switch.

This switching tree was calibrated once, after fabrication. With high-intensity blue light, however, we encountered material instability, which resulted in fractions of light leaking from undesired emitters and thus required recalibration. We managed this issue by limiting the power of blue light. Therefore, in experiments requiring high light intensity and precise spatial addressing, we used red light.

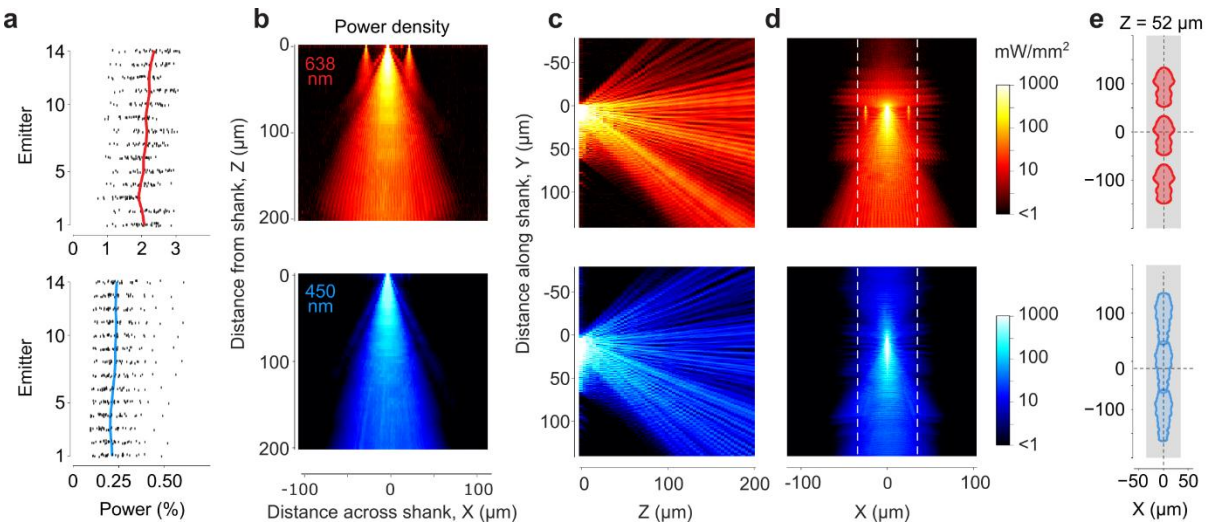

Figure 2 – Optical characterization of the Neuropixels Opto probe. **a**, Efficiency of the emitters, showing output light power as a percentage of input power for 14 red (*top*) and blue (*bottom*) emitters from N = 14 probes. Curves show average over probes. **b**, Top view, showing light propagation from a red and blue emitter, measured in water. The color (color scale in panel d) indicates the max projection. These measurements were made on a test structure where emitters were placed 25 µm apart rather than the 100 µm of the prototype probe (Methods) and this led to small imaging artifacts visible in the red emission (*top*), where two emitters to the side of the central one also appear to emit light. **c**, Same data, projected over a side view. **d**, Same data, projected over a front view. Dashed lines delineate the width of the probe. **e**, Section on a plane located 52 µm away from the shank, showing areas where power density is >10 mW/mm^2 (for a 100 µW output) for three nearby emitters.

The package includes a CMOS circuit mounted on a flexible printed circuit board (PCB ,**Figure 1d**). To accommodate the fiber block and the photonics circuitry, we extended the 5-mm probe base integrating the recording circuits with two wings of 2 and 3 mm. The probe transmits data via flex cable to a headstage PCB, which connects to a digital data cable.

The data cable and the two-channel optical fiber cable are connected to two modules in a PXI base station, one for digital data processing and one containing blue and red lasers (**Figure 1e**). Data acquisition, light delivery, and emitter selection are controlled by one of two widely used open-source software packages: SpikeGLX[1] and Open Ephys GUI[56], which were updated for the purpose.

Electrical and optical characterization

Despite the addition of the photonics, the electrical performance of the Neuropixels Opto probe remained similar to the widely used Neuropixels 1.0 probes[1]. The average impedance was 138 ± 27 kΩ, and the average RMS noise in the AP and LFP bands was 5.4 ± 2.4 μV and 5.3 ± 3.7 μV (**Supplementary Figure S2**). This low noise, combined with high site density (100 sites/mm), enables recordings with similar yields as those routinely obtained with established Neuropixels probes.

As expected, the light at the emitters was a small fraction of the light delivered by the optical fibers: the average emitted power was ~2% of the input power for red light, and ~0.25% for blue light (**Figure 2a**). The attenuation (–16.9 ± 1.2 dB for red, –26.4 ± 1.6 dB for blue) is caused by the coupling of fiber to waveguide (~6 dB), the switching tree (~4 dB), the emission site (simulated < 4 dB) and waveguide propagation, where losses are particularly strong with blue light (3.0 dB/cm, compared to 0.5 dB/cm for red light). Because of these losses, achieving 100 μW of output at the emitters requires input powers of ~5 mW for the red light and ~40 mW for the blue light. These powers are easily delivered by external lasers.

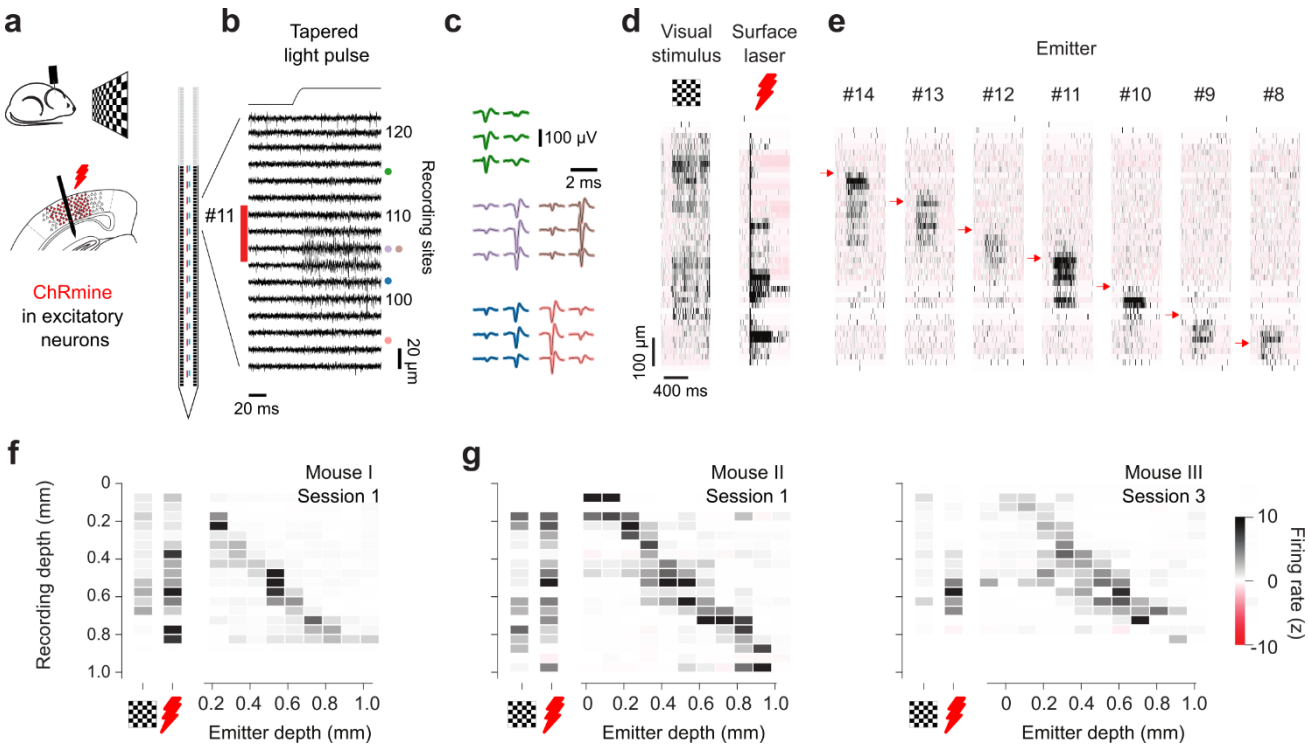

Figure 3 – Using Neuropixels Opto to record and activate localized neural populations. a. We inserted a Neuropixels Opto probe ~1.4 mm deep in the visual cortex of a mouse expressing the red-sensitive opsin ChRmine in cortical excitatory neurons (via a virus with CaMK2 promoter). Mice viewed a visual stimulus, and an additional red laser could illuminate the surface of the posterior cortex. **b**. Simultaneous Neuropixels Opto recordings and optical stimulation with an example emitter (#11). Recordings (while the screen was gray, with no external laser), show baseline activity 50 ms prior to emitter photostimulation and strong spiking activity after stimulation onset on a subset of recordings sites near emitter 11. **c**. Average spike waveforms from five example single units recorded on sites near emitter 11. The mean waveform was calculated across 100 spikes. **d**. Average firing rate (bin size 50 µm, 10 trials) for the same recording session, plotted as a function of depth, showing cortical responses to visual stimulation and surface illumination. Color scale bar appears at the bottom right of the figure. **e**. Responses of the same neurons to single emitter activations at different depths (*arrows*). **f**. Summary of these data showing average over time of response during stimulation with visual stimulus, surface laser, and single emitters (abscissa), at different cortical depths (ordinate). **g**. Same format, for example sessions in two other mice. Additional measurements in these mice are shown in Supplementary Figure S3.

The emitted light is sufficient for optogenetic manipulations of neurons in the vicinity of the probe (**Figure 2b-d**). For ChR2, estimates of the light intensity required for optogenetic stimulation range from 10 mW/mm^2 (Ref. [50]) to 5 mW/mm^2 (Ref. [57]) to 1 mW/mm^2 (Ref. [58]). The variability perhaps reflects differences in preparations, opsin expression levels, and spatial overlap of excitation light with the neuron's membrane. To be conservative we used the higher estimates, and measured the volume where light power density is at least 10 mW/mm^2. For a 100 μW output, this volume exceeds 470,000 μm^3, extending >100 μm from the shank over a wide angular range (**Figure 2b-c**). This is more than sufficient to stimulate neurons in the vicinity of the recording sites and beyond the ~50 μm limit for single-unit recordings[59,60]. The volume where light power density is >1 mW/mm^2 is considerably larger, and exceeds the range of the microscope used for these measurements. Moreover, this volume is expected to be homogenous, as the diffraction patterns (which were here measured in water) will be blurred by light scattering in brain tissue.

The close spacing of the emitters means that there is a minimal gap between the patterns of light emitted by different emitters: when slicing the emission profile close to the shank (in a plane

~50 μm away), the area with a power density >10 mW/mm^2 largely tiles the shank axis (**Figure 2e**).

Activating local neural populations

The probes were able to activate spatially separated neuronal populations. We inserted Neuropixels Opto probes acutely in the primary visual cortex of awake, head-fixed mice following local viral expression of the red-sensitive depolarizing opsin ChRmine[48] in excitatory (CaMK2$^+$) cells of the visual cortex (**Figure 3a**). Tapered pulses of red light (638 nm) lasting 400 ms at one example emitter elicited neural activity that was restricted to recording sites near the emitter (**Figure 3b**). These recordings had similar quality to standard Neuropixels probes[1,2]. We could then readily spike-sort them to obtain the spikes of individual neurons (**Figure 3c**) and summarize this activity in terms of firing rate as a function of cortical depth (**Figure 3d**). To establish baseline measurements, we then presented a visual stimulus (full-field checkerboard) and we illuminated the surface of the posterior cortex with a red laser (638 nm, 5 mW). These baseline measurements indicated the presence of recordable neurons throughout the depth of the cortex.

By activating one emitter at a time, Neuropixels Opto probes could spatially address different subpopulations of these neurons with high resolution (**Figure 3e**). Trials with stimulation from different emitters were randomized and randomly interleaved with the baseline trials (visual stimulus or surface laser). Stimulation by single emitters activated smaller groups of these neurons at nearby depths. Taking the average over time of these responses revealed an approximately diagonal matrix (**Figure 3f**), reflecting concordance between the location of stimulation and the location of neurons with increased firing rates. Similar results were obtained in two other mice (**Figure 3g**) and across multiple experiments (**Supplementary Figure S3**). These results indicate that Neuropixels Opto probes provide concurrent large-scale recordings and fine spatially addressed optogenetics across the depth of a brain structure.

Driving localized network effects

We next tested the ability of Neuropixels Opto probes to drive network effects such as those mediated by synaptic inhibition. We expressed the red-sensitive depolarizing opsin Chrimson[47] in forebrain inhibitory neurons by systemic viral injection[61]. We then inserted Neuropixels Opto probes in the visual or motor cortex of awake, head-fixed mice, and we delivered 250 ms pulses of light at random times from random emitters.

The results revealed localized activation of inhibitory neurons and inactivation of excitatory neurons. Light delivery activated some neurons and inactivated others (**Figure 4a-d**). Because the opsin depolarizes neurons in which it is expressed, the activated neurons should correspond to inhibitory neurons expressing the opsin, while inactivated neurons could only reflect neurons receiving synaptic inhibition from the activated population. To test this interpretation, we analyzed the spike waveforms[62] and distinguished putative fast-spiking inhibitory neurons, which have narrow spikes, from the rest of the neurons, which are likely to be mostly pyramidal and have broader spikes[63]. As expected[62], the activated neurons were predominantly fast-spiking, whereas the putative pyramidal neurons were predominantly inactivated. Moreover, cross-correlograms[63,64] between some pairs of activated and inactivated neurons were consistent with monosynaptic inhibitory connections (**Figure 4f**). Both activated and inactivated neurons were observed primarily at depths near the emitter (**Figure 4g**), indicating that the localized activation of inhibitory neurons engaged localized network effects. These results confirm that Neuropixels Opto probes are suitable for causing spatially-localized circuit effects mediated by synaptic transmission.

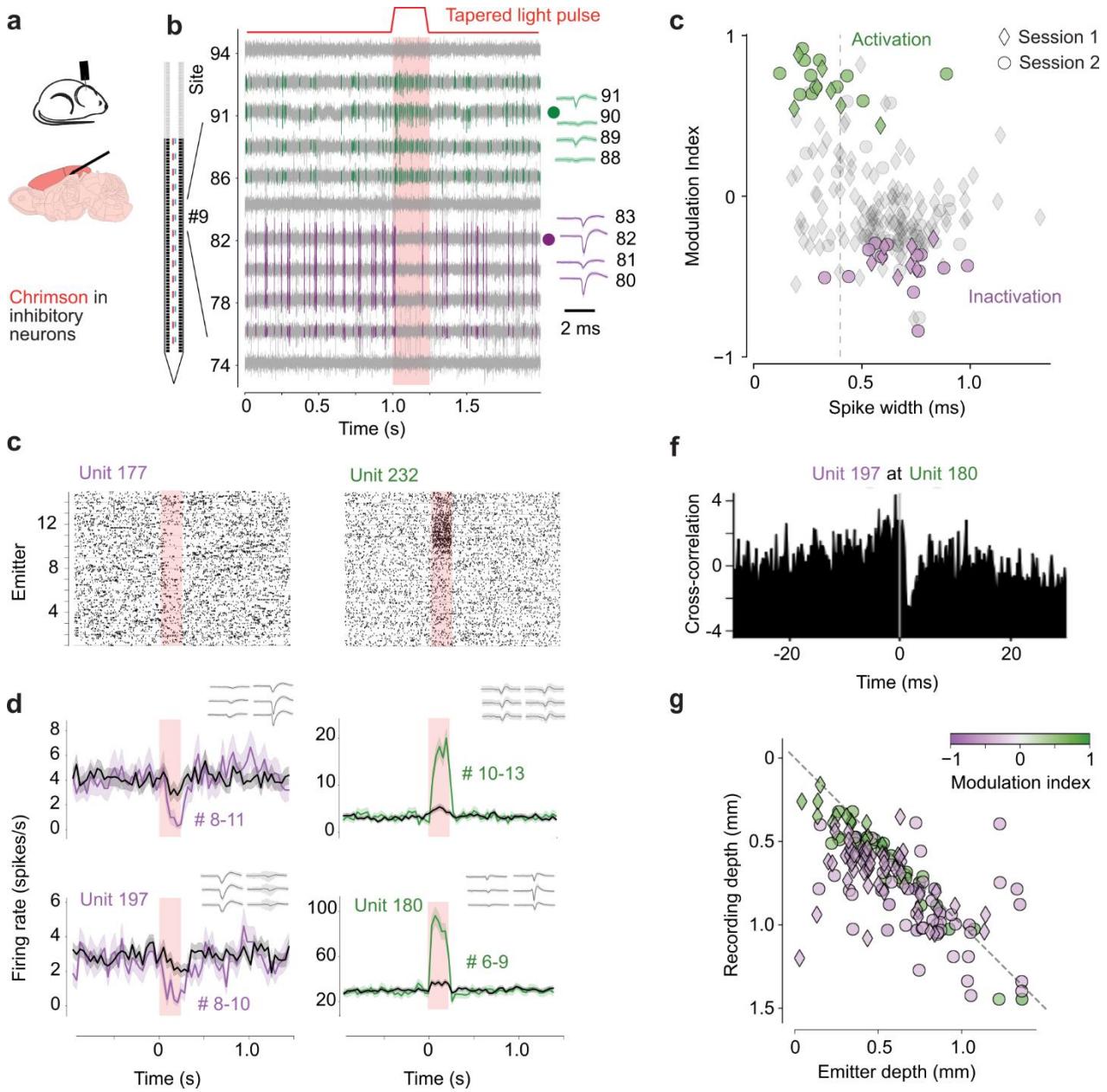

Figure 4 – Using Neuropixels Opto to drive localized network effects. **a**. We inserted a Neuropixels Opto probe in the motor or visual cortex of a mouse expressing red-sensitive depolarizing opsin Chrimson in inhibitory neurons (via Dlx2 enhancer virus). **b**. Electrical signals at 20 recording sites during red light stimulation from emitter 9. Colors indicate the spikes of two nearby units, one activated (unit 189, *green*) and one inactivated (unit 208, *purple*) by light. Waveforms across peak channels (*right*) confirm neural activity. **c**. Spike rasters for a pair of example units, one inactivated (unit 177) and one activated (unit 232) by light. **d**. Average firing rate (40 ms bin size) relative to light onset for those units and for two additional units (197 and 180). Shading indicates ±1 s.e. Waveforms (*insets*) show spike shapes across 6 peak recordings sites. **e**. Spike width (trough to peak) of average waveforms vs. effect of light stimulation, measured by a modulation index $(R_1-R_0)/(R_1+R_0)$ where R_0 and R_1 are firing rates before and during stimulus, showing significantly activated units (*green*) and inactivated units (*purple*) at $p < 0.05$ (paired t-test). Narrow spikes were defined as width < 0.4 ms (*vertical line*). **f**. Cross-correlogram between units 197 and 180. **g**. Recording vs. emitter depth for significantly modulated neurons. Each neuron appears at one recording depth and at one or more emitter depths (if modulated by light from multiple emitters).

Optotagging nearby neurons

When light-sensitive opsins are expressed in a cell-type-specific manner, these cells can be identified in extracellular recordings via optotagging[3-5], i.e. based on their low-latency responses to pulses of light. An ideal tool for optotagging would have minimal artifacts in response to light pulses, minimal activation of neurons outside the range of recording, and the ability to deliver both blue and red light wavelengths deep inside the brain. These criteria are all met by Neuropixels Opto probes. By incorporating emitters into the shank, they localize light to the volume of interest while directing it away from the recording sites.

By delivering light away from the recording sites, Neuropixels Opto probes largely avoid photoelectric artifacts. Illumination of Neuropixels recording sites with sharp-onset surface stimulation creates a photoelectric artifact in the range of 1 mV or more[1]. By contrast, illumination via Neuropixels Opto emitters caused a small artifact of ~30 μV (present only with red light), which was uniform across recording sites and easily canceled with standard preprocessing steps (**Supplementary Figure S4**).

Thanks to these favorable properties, Neuropixels Opto probes performed well in recording and dual-color tagging pairs of cell populations in deep structures. We demonstrated this ability by tagging direct-pathway and indirect-pathway medium spiny neurons (MSN) in the dorsal striatum using blue and red light. We expressed the blue-sensitive opsin CoChR[47] in D1 MSNs (direct pathway) with an enhancer AAV virus[65], and the red-sensitive opsin ChRmine[48] in D2 MSNs (indirect pathway) via a Cre-dependent AAV in a specific (Adora2a-Cre) driver line (**Figure 5a**, see Methods for virus details). Because the photoartifacts were small and disappeared after preprocessing, spikes were readily identifiable in the raw traces around each light pulse (**Figure 5b**). For example, consider two units tagged by red light pulses from emitter 3 (**Figure 5c**). Each unit shows consistent, low-latency spiking responses to each of five 100 μW pulses across 50 trials (**Figure 5d**).

When aggregating across all emitters, the strongest responses were evoked by the emitter near the estimated position of the soma (**Figure 5e**). For units tagged with blue light, some longer-latency spikes were evoked also by emitters distant from the soma, perhaps due to the small amounts of light leakage mentioned earlier (which are specific to blue light and would require recalibration). In this recording, we were able to tag most units in striatum passing quality control (43 out of 67) (**Figure 5f**), allowing direct comparison of the activity of populations of two cell types in a single structure.

Similar results were obtained in other subcortical regions and with other opsins. Overall, we optotagged 302 units in striatum, globus pallidus, and midbrain reticular nucleus (34 sessions in 23 mice). In these sessions, we successfully tested various combinations of opsins: in addition to CoChR[47] and ChRmine[48], we used ChrimsonR[47], rsChRmine[66], and somBiPOLES[67] (**Supplementary Table 1**).

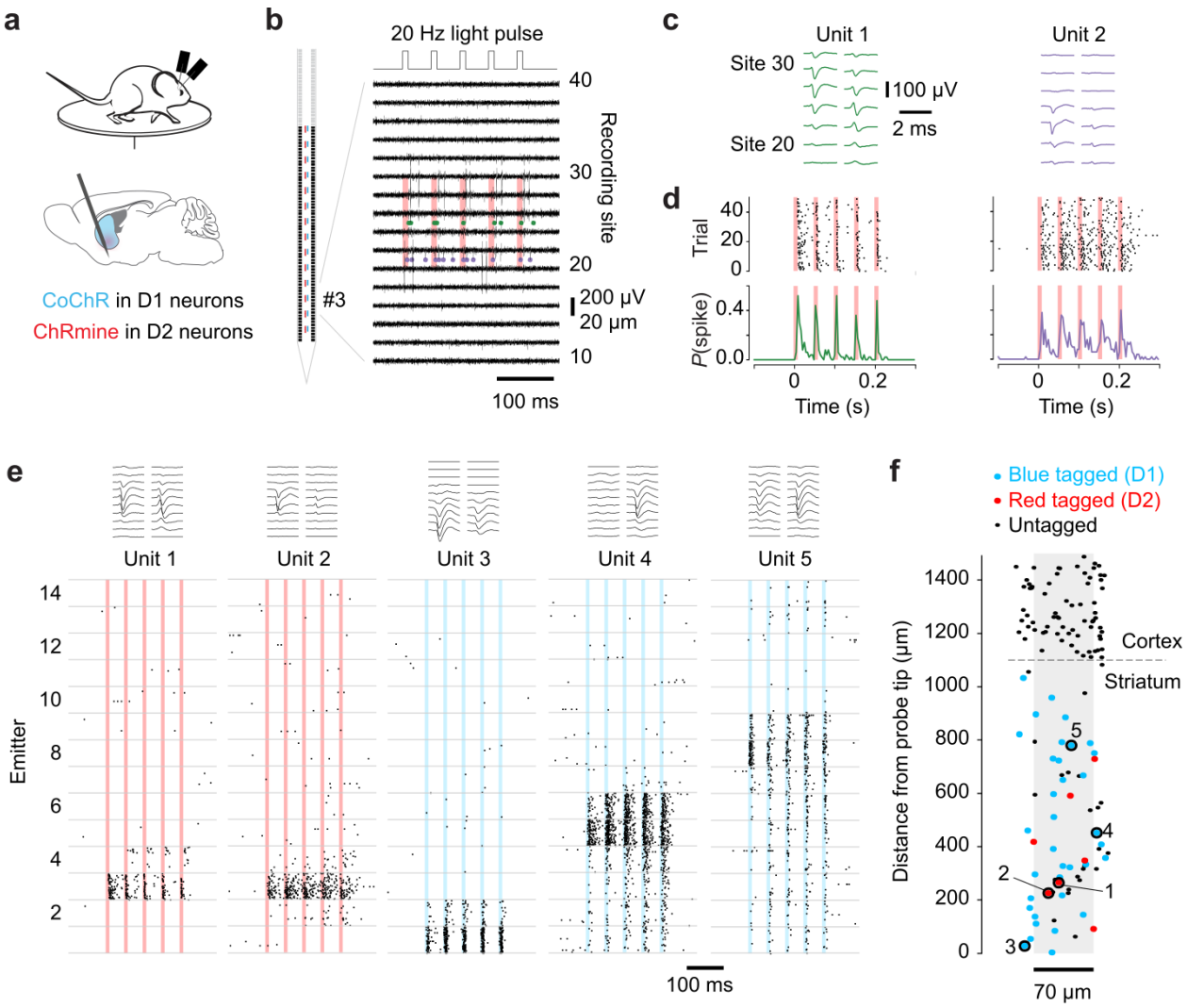

Figure 5 – Using Neuropixels Opto for optotagging. a, We inserted two Neuropixels Opto probes in the striatum of Adora2a-Cre mice expressing the blue-sensitive opsin CoChR in D1-MSNs (via a D1-MSN specific enhancer virus) and the red-sensitive opsin ChRmine in D2 MSNs (via a Cre-dependent AAV). Mice were free to run on a disc. After 20 min recording we ran the optotagging protocol (10 ms, 20 Hz, 100 µW pulses from each of 14 blue or red emitters, randomly interleaved). **b**, Recorded traces around the time of stimulation, showing spike times (green and red dots) of two example units tagged by red light from emitter 3. **c**, Mean waveforms for the two units. **d**, Spike raster and peri-stimulus time histogram for 50 trials of stimulation from emitter 3, showing consistent, low-latency response to each light pulse. **e**, Stacked rasters across 50 trials from all 14 emitters for five example units (including the two units from panels b–d). **f**, Estimated location of all units passing quality control from a single recording, with units activated by blue or red light shown in blue and units activated by red light only shown in red.

By combining these measurements, we confirmed that the emitters provide uniform optogenetic coverage. We estimated the location of every unit (based on the spatial distribution of its spike waveform), and compared the position of optotagged and untagged units (**Figure 6a,b**). We expressed each unit's position relative to the driving emitter (the emitter evoking the most low-latency spikes), and found that optotagged units tended to be lower than the driving emitter (**Figure 6c**). This arrangement is consistent with the illumination profile (**Figure 2e)**. We then plotted each unit's position relative to the *nearest* emitter, whether or not this emitter evoked any spikes (**Figure 6d**). Along the width of the shank, tagged units tended to lie near the centerline (**Figure 6e**). Along the length of the shank, tagged units were distributed evenly: the 100 µm between them is sufficient to leave no gaps in coverage (**Figure 6f**).

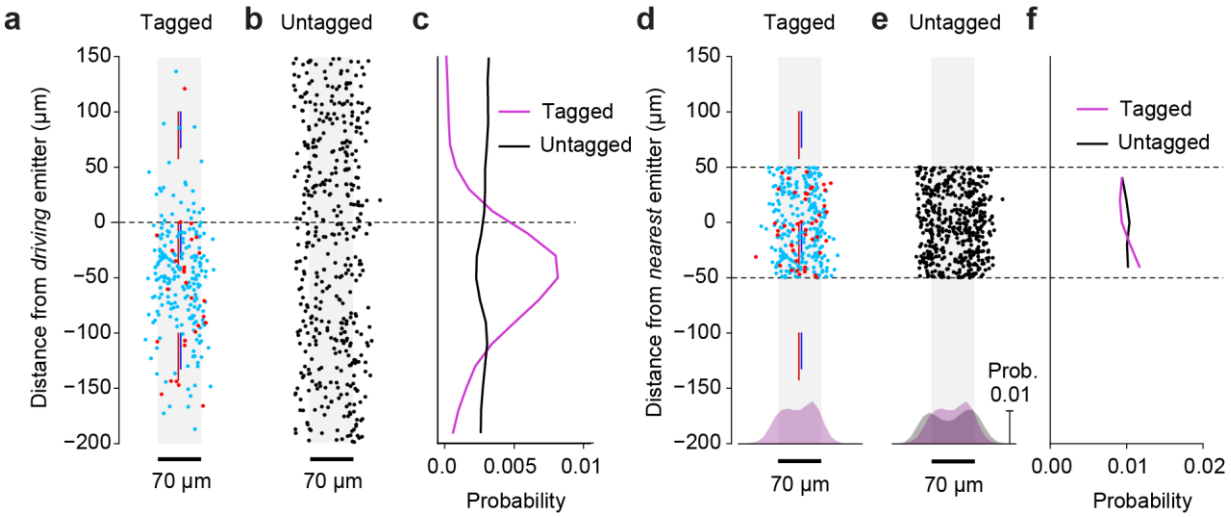

Figure 6 – Spatial distribution of optotagged units. a, Estimated location of units relative to the driving emitter, for units that were optotagged by red light (*red dots*, *N* = 50 units from 15 sessions) and blue light (*blue dots*, *N* = 252 units from 30 sessions). **b**, Same as panel a, but for units from the same sessions that were not optotagged (*black dots, N* = 500 randomly selected units from 34 sessions). For these untagged units, the driving emitter is selected arbitrarily. **c,** Probability of tagging a unit as a function of distance from the driving emitter along the shank insertion axis. Most tagged units are located below the driving emitter (deeper in the brain). **d-f**, Same data as panels a-c, plotted relative to the nearest emitter (rather than the driving emitter), showing that units have a similar probability of being optotagged at any location within 50 µm of an emitter. The histograms at the bottom of d and e show the distributions of unit locations orthogonal to the shank insertion axis. See **Supplementary Table 1** for information about cell types and opsins in these experiments.

Discussion

Thanks to integrated CMOS and photonics, Neuropixels Opto probes provide a single device for large-scale neural recordings and spatially addressable optogenetics. Our tests demonstrate that these probes can precisely manipulate neural activity near emitters in the intact brain. They thus deliver fine spatially-addressable optogenetics across the depth of a brain structure, while providing high-resolution, large-scale recordings. This capability is unprecedented, and is ideal for investigating the circuit organization of the cerebral cortex[7,14-17] and other brain regions. In addition, Neuropixels Opto is well-suited for optotagging[3-5], making it possible, for the first time, to identify the cell type of the majority of units in regions such as the striatum.

As with Neuropixels 1.0 and 2.0 probes[1,2], our model is to produce the Neuropixels Opto probes in quantity and distribute them at cost to a wide community. Here we have demonstrated successful prototype probes. Turning these prototype probes into a mass-producible probe requires additional rounds of fabrication and testing. As with the 1.0 and 2.0 probes, during this process we may further adjust the design. For instance, we aim to make the blue-light switches and waveguides more robust by putting them in a separate photonic layer. We may also simplify the coupling between lasers and probe, and reduce the probe's form factor, by upgrading the CMOS backend to the more compact design developed for the 2.0 probes[2]. Finally, it may be possible to increase the number of red and blue emitters.

We anticipate that Neuropixels Opto probes will become an essential tool for combining high-density electrophysiological recordings with local optogenetic activation or inactivation, and for cell type-specific electrophysiology across the brain.

Acknowledgments

We thank numerous colleagues who contributed to this project. At IMEC, Enrico Tonon contributed invaluable assistance. At UCL, Charu Reddy, Bex Terry, and Magdalena Robacha assisted with lab management, colony management, and brain sectioning. At UW, Ljuvica Kolich and Kimberly Miller assisted with mouse husbandry. At AI, the Allen Institute Transgenic Colony Management, Lab Animal Services, Neurosurgery & Behavior Team, and Viral Core provided invaluable assistance, Ximena Opitz-Araya managed cloning of viral vectors, and Alessio Buccino helped with spike sorting pipelines. This research was funded by the Wellcome Trust (grants 204915/Z/16/Z to MC, MH, and TDH and 225819/Z/22/Z to MC, MH, and NAS), the Howard Hughes Medical Institute (TDH), the BRAIN Initiative (U01NS133760 to JHS and KS; UF1MH128339 to JT), the Paul G Allen Family Foundation (CK, JHS and KS), the Research Council of Norway (NORBRAIN 350201 to EIM), the Pew Biomedical Scholars Program (NAS), and the Klingenstein-Simons Fellowship in Neuroscience (NAS). MC holds the GlaxoSmithKline / Fight for Sight Chair in Visual Neuroscience.

Consortium membership

The Neuropixels Opto Consortium includes Matteo Carandini (UCL), Barun Dutta (IMEC), Timothy D Harris (HHMI and JHU), Michael Häusser (UCL), Sonja Hofer (UCL), Edvard I Moser (NTNU), Josh Siegle (AI), Nicholas Steinmetz (UW), and Karel Svoboda (AI).

Author contributions

	Bowen	Carandini	Chen	Colonell	Doshi	Dutta	Harris	Häusser	Karsh	Koch	Krumin	Kulik	Ladd	Lakunina	Li	Neutens	O'Callaghan	Olsen	Putzeys	Siegle	Socha	Steinmetz	Svoboda	Tilmans	Ting	Ye	Welkenhuysen
Conceptualization		✱				✱	✱													✱		✱	✱				
Data curation													✱	✱		✱					✱						
Formal analysis											✱		✱	✱						✱	✱						
Funding acquisition		✱					✱	✱		✱										✱		✱	✱				
Investigation	✱		✱										✱	✱	✱	✱		✱			✱					✱	
Methodology						✱					✱					✱	✱		✱	✱			✱	✱			✱
Project administration		✱				✱														✱							
Software				✱	✱				✱		✱	✱								✱							
Resources		✱				✱	✱													✱		✱	✱		✱		
Supervision		✱				✱	✱	✱		✱										✱		✱	✱				
Validation				✱					✱												✱						
Visualization		✱											✱	✱						✱	✱						
Writing – original draft		✱											✱							✱	✱	✱					
Writing – review & editing		✱											✱	✱		✱				✱	✱	✱	✱				

Author contributions according to the CRediT taxonomy.

Methods

Light source

Except where indicated, the light source was a PXI-mounted laser module emitting light at 450 nm and 638nm (Quantifi Photonics, New Zealand), connected to the Neuropixels Opto probe via an optic fiber. After the electrical characterization measurements, the light power was calibrated based on the measured loss for each emitter, such that the output levels were consistent across emitters.

Electrical and optical characterization

The electrical and optical characterizations (**Supplementary Figure S2**, **Figure 2**) were performed at IMEC.

Electrical characterization. Measurements were performed in a grounded Faraday cage. The probe shank was immersed in phosphate-buffered saline (PBS) solution. The channels were configured to use external reference and x1000 gain. The external reference input was connected to the ground pad of the probe. First, we measured gain. We applied a sinusoidal test signal of 500 µV (peak to peak) at 1.5 kHz or 150 Hz (for AP or LFP band) to the PBS solution using a platinum (Pt) counter electrode. We recorded the probe signal and calculated the gain at the two frequencies. Second, we measured noise. We grounded the PBS solution via the external reference and ground contact pads on the flex cable. We recorded the probe signal and we calculated the integrated noise in the frequency bands for AP and LFP. We then divided the measured noise by the measured gain to obtain the input-referred noise.

Optical characterization. To measure the emitter radiation pattern, we used a Nikon Eclipse microscope with a water immersion objective (Nikon Fluor, 60X/1.0NA), and a motorized 3D fiber coupling stage (based on the PI Q-545 linear stage). Images were acquired with a scientific CMOS camera (Hamamatsu Orca Flash) providing a field of view of 220 x 220 µm. To perform the measurement, the microscope field of view was centered on the emitter, and the objective was focused on the waveguide plane. A 200 µm z-scan was performed with a 4 µm step, and the imaged frames were saved into a 3D matrix.

These measurements were made on a test structure: a 1 cm long waveguide with a standard grating coupler on one side, and the emitter on the other side. Light was coupled into the structure with a horizontally placed 40 deg angle polished fiber, which was actively aligned to the standard grating coupler. The test structures were arranged in large blocks with many waveguides next to each other on a 25 µm pitch. For red light, we could not avoid coupling some light into the neighboring waveguides, resulting in small artifacts where a small amount of light was visible in neighboring emitters (**Figure 2b**, *top*). These artifacts were specific to the test structure layout and the properties of the fiber coupling. They were not present at the emitters of fully constructed probes.

Activating local neural populations

The experiments demonstrating recording and activation of local neural populations (**Figure 3, Supplementary Figure S3**) were performed at University College London. Experimental procedures were conducted according to the UK Animals Scientific Procedures Act (1986) under personal and project licenses released by the Home Office following appropriate ethics review.

Mice and viral strategy. The experiments described here were performed on 3 adult mice (aged 10-16 weeks at the time of headplate implantation): one male with wildtype background (C57BL/6, Charles

River) and two females with double-transgenic background (Ai32[68] x PV-Cre[69], JAX #012569 and #008069). The 2 transgenic mice expressed the blue-sensitive opsin ChR2 in inhibitory (PV+) neurons. For the measurements presented here, all 3 mice were injected with a virus expressing red-sensitive opsin ChRmine in excitatory (CaMK2+) neurons[48] (AAV-8-CaMKIIa-ChRmine-eYFP-Kv2.1-WPRE, #GVVC-AAV-196)

Main surgery. An initial surgery was performed to implant a headplate, perform a craniotomy, and inject a virus. Procedures were adapted from an established protocol[70]. Briefly, mice were injected with dexamethasone (i.m.) before surgery, and then anesthetized with isoflurane (3% for induction; 1–1.5% for maintenance). Appropriate hydration and temperature control were provided. A steel headplate was attached to the skull and secured with dental cement (Super-Bond C&B, Sun Medical Co). The skin margins were attached to the cranium with tissue adhesive (Vetbond, 3M). A 3 mm craniotomy was performed, centered on the left primary visual area (VISp, ~3.7 mm posterior and ~3 mm lateral from bregma). A glass pipette (Drummond Scientific), beveled to form a ~25-40 µm tip (EG-45 Microgrinder, Narishige), was lowered stereotaxically 150, 300, and 550 µm into the brain, to deliver 70 nL of viral vector solution (diluted 1:5) at each depth (Nanoject II, Drummond Scientific), with 3 min pauses between depths, and a 5 min pause at the bottom. Injections were performed in 4-5 locations in VISp, 500-750 µm apart. The total volume of virus solution delivered was 840-1050 nL. The craniotomy was then covered with a removable window[71] comprising two 3-mm circular cover glasses (#1) attached to a 5-mm circular cover glass (#1, Warner Instruments) using optical adhesive (Norland Optical Adhesive NOA 61, Thorlabs). The remaining exposed cranium and the skin margin were covered with cement (Super-Bond C&B). Post-operative treatment was provided for 3 days with carprofen in drinking water. Later, the mice were handled and habituated to the head-fixed recording rig for 30-60 min for at least 4 days before any recordings.

Widefield imaging. We waited 3–4 weeks for the virus to fully express and found the locations of virus expression using epi-fluorescence widefield imaging involving an illuminator (X-Cite DC200, Excelitas, Canada), a trinocular (Nikon C-TF), a 4x 0.13 NA air objective (UPlanFL N, Olympus), filter cubes for GFP and TurboFP635 (Chroma, VT), and a sCMOS camera (PCO.Edge 5.5 CLHS, Excelitas Canada Inc.). We then prepared a replacement glass window with holes in the appropriate locations.

Window replacement. To replace the glass window with one that had drilled holes At least 12 hours before the first recordings, we performed a brief procedure to replace the glass window. Mice were anesthetized using isoflurane (3% for induction; 1–1.5% for maintenance). The cement around the glass window was removed with a dental drill, and the new window was implanted in its place. We made an incision in the dura at the recording site to allow easier probe insertion, then covered the craniotomy with artificial dura[72] (Duragel, Cambridge NeuroTech) and sealed the holes with Kwik-Cast (WPI, USA).

Recordings. A Neuropixels Opto probe with metal dovetail was mounted on a HHMI-designed probe holder and then on a 4-axis micromanipulator (uMp-4, Sensapex). In some recordings, we labeled the probe tip using Vybrant CM-DiI or DiO (V22888 or V22886, ThermoFisher). We lowered the probe to the brain surface and inserted it at 2 µm/s, typically reaching a depth of 1.2-1.4 mm. We then waited 15 min for the probe to settle, and started the recordings. During recordings, we controlled the probe and acquired signals using SpikeGLX, with standard gain settings of 500x and 250x for the AP and LFP bands. After recordings, we sealed the hole in the glass window with Kwik-Cast, and we cleaned the probes by placing the shank in distilled water overnight. Occasionally, the probes required additional cleaning due to Duragel or tissue sticking to the shank; they were rinsed with a 1% Tergazyme solution for 30 min before being moved to distilled water.

Photostimulation. Pulses of light had a smooth onset, ramping from 0 with half a cycle of a 40 Hz sine wave, and lasted 400 ms. The pulses were randomized across the 14 emitters, randomly interleaved with control trials (external illumination, visual stimulation, and gray screen), and repeated 40 times. The average inter-trial interval was 1 s. External optical activation was done using a 638 nm diode laser (LuxX 638-150, Omicron-Laserage Laserproducte, Germany). The laser light was delivered to the brain surface using a 200 mm, 0.22 NA patch cord (M122L02, Thorlabs), a collimator (F280FC-A, Thorlabs), and a focusing lens (f = 50mm, LA1213-A, Thorlabs) positioned ~5 cm above the brain surface. Visual stimulation (full-field flickering checkerboard, 100% contrast, 1s) was displayed on an LCD screen (LP097Qx1, LG).

Postprocessing. We used Kilosort 2.5 for spike sorting, and curated the results with Phy to isolate multi-unit and single unit activity.

Histology. Following the recordings, the mice were perfused with 4% PFA (#28908, ThermoFisher). The brain was dissected and post-fixed in PFA for 24 hours. Then, the brain was stored in 10% PBS for at least 48 hours before sectioning. We imaged full 3D stacks of the brains in a custom-made serial section two-photon tomography microscope[73]. Images were acquired using ScanImage (Vidrio Technologies) and the hardware was coordinated with BakingTray.

Driving localized network effects

The spatially resolved neural inactivations (**Figure 4**) were performed at the University of Washington.

Mice and viral strategy. The experiments described here were performed on 1 adult female mouse (aged 19 weeks at the time of headplate implantation) with transgenic background (CaMK2a-tTA.tetO-G8s). Mice were injected with a virus expressing red-sensitive opsin ChrimsonR in inhibitory neurons[74] (AAV-PHP.eB-DLX2.0-ChrimsonR-tdTomato, Addgene plasmid #229775). The virus was injected retro-orbitally in anesthetized (isoflurane 1-4% in O2) 4–6-week-old mice.

Implant surgery. Implant surgeries were performed after mice reached p48 or later. Mice anesthetized with isoflurane (1-4% in O2) and subcutaneously administered analgesics carprofen (5 mg/kg) and lidocaine (2 mg/kg). The skin and periosteum were cleared to reveal the dorsal skull. The edges of the implant were sealed to the skull then secured to the skull with cyanoacrylate (VetBond, World Precision Instruments) to protect the underlying muscle. A 3-D printed recording chamber was implanted on top of the skull using dental cement (Metabond, Parkell). Fast-curing optical adhesive (Norland Optical Adhesive 81, Norland Products) was applied to the surface of the skull and cured with UV light. A titanium headpost (ProtoLabs) was then cemented to the posterior end of the recording chamber. Carprofen (0.05 mg/ml) was given for 2 days in water after surgery. Mice were allowed to recover in the home cage for at least one week before habituation and head-fixation.

Recordings. Over 3 hours before a recording session, the mouse was anesthetized (isoflurane 1-4% in O2) and a 2-3 mm craniotomy was performed over the left visual cortex and right motor cortex. Craniotomies were sealed with transparent Duragel (Dow Corning 3-4680 Silicone Gel). After recovery from anesthesia, mice were head-fixed. The Neuropixels Opto probe was mounted on a micromanipulator and manually driven to the craniotomy at a 45° angle to accommodate an overhead laser. Real-time electrophysiological data was monitored as the probe was driven through into the brain. Insertions aimed to avoid blood vessels. If a probe could not successfully record from a craniotomy, a new surgery was performed at a later date. Once probes reached the brain's surface, they were driven to their target depth at 200 µm/min. Probes were allowed to settle for 10 min at their final depth before recording data with SpikeGLX. We used internal tip referencing with gain settings of 1000x and 1000x for the AP and LFP

bands. Probes were slowly removed from the brain (~1 mm/min) at the end of recording. Probes were submerged in a 1% Tergazyme solution overnight and then rinsed in deionized water the next day to clean debris off the shank of the probe.

Photostimulation. To activate and inactivate neurons with light emitted from the probe, we presented a 250 ms tapered square pulse of red light (638 nm) from a randomly chosen emitter with an average inter-trial interval of 1.4 s. The square pulse is tapered as the signal ramps up linearly for the first 25ms and then ramps down for the last 25 ms.

Data processing. We used SpikeInterface[75] to preprocess the raw data (decompression, phase shift, high-pass filter, and median subtraction). We then used Kilosort 4 (Ref. [76]) for spike sorting. A range of quality metrics (including ISI violations ratio, amplitude cutoff, and presence ratio) were calculated for each unit. We used Neuropyxels[77] to plot raw waveforms from SpikeGLX data. Light-activated neuron-emitter pairs were defined by a >300% increase in firing rate during the 250 ms light stimulus compared to the pre-stimulus baseline with $p < 0.05$. Inactivated neuron-emitter pairs were identified as having at least a 50% reduction in firing rate during the stimulus period with $p < 0.05$. Modulation index was computed as (R1-R0)/(R1+R0) where R0 and R1 are mean firing rates before and during stimulus. When calculating modulation index (**Figure 4e**), we averaged the mean firing rates (R0 and R1) for the two most proximal emitters superficial to each unit.

Optotagging nearby neurons

The subcortical optotagging experiments (**Figure 5** and **Figure 6**) were carried out at the Allen Institute, in accordance with protocols approved by the Institutional Animal Care and Use Committee (IACUC).

Mice and viral strategy. Experiments were performed on 23 adult mice (10 males, 13 females; aged 16-34 weeks at the time of headframe implantation). We used eight transgenic lines:

- Chat-IRES-Cre[78] (JAX #031661)
- Chat-IRES-Cre-neo[78] (JAX #006410)
- Sst-IRES-Cre (JAX #028864)
- Drd1a-Cre[79] (JAX #037156)
- Adora2a-Cre (MMRRC #36158)
- Slc17a6-IRES-Cre[80] (JAX #028863)
- Ntrk1-IRES-Cre (MMRRC #15500)
- Gad2-IRES-Cre[81] (JAX #028867)

In addition, some mice received one or more of the following viral injections (as described below):

- pAAV-Syn-FLEX-rc(ChrimsonR-tdTomato) (Addgene #62723)
- pAAV-Ef1a-DIO-ChRmine-mScarlet-WPRE (Addgene #130998)
- pAAV-Ef1a-DIO-rsChRmine-oScarlet-Kv2.1-WPRE (Addgene #183529)
- hSyn-DIO-somBiPOLES-mCerulean (Addgene #154951)
- AiP14033: pAAV-AiE0779m_3xC2-minBG-CoChR-EGFP-WPRE3-BGHpA (Addgene #214852)
- AiP14035: pAAV-AiE0452h_3xC2-minBG-CoChR-EGFP-WPRE3-BGHpA (Addgene #214853)
- AiP14036: pAAV-AiE0743m_3xC2-minBG-CoChR-EGFP-WPRE3-BGHpA (Addgene #214854)

The example experiment (**Figure 5**) involved Adora2a-Cre mice (MMRRC #36158) injected with viruses expressing CoChR-EGFP (Addgene #214852) and ChRmine-mScarlet (AAV-PHP.eB-DIO-ChRmine).

Surgery. Mice were anesthetized and placed in a stereotaxic frame. The dorsal scalp was removed, the skull leveled, and bregma located using tooling adapted from a previously described headframe and clamping system[82]. An outline of the implant location was etched using a custom tracing tool, and the assembled headframe was cemented in place. A craniotomy was performed using the traced implant shape as a guide, and the dura was removed. If the mouse was to receive viral injections, these were delivered stereotaxically through the craniotomy. Afterwards, the prepared 3D-printed SHIELD artificial skull[83] was placed in the opening. The edges of the implant were sealed to the skull using a light curing cyanoacrylate adhesive (Loctite 4305) and reinforced with dental cement. Finally, a removable plastic cap was placed over the well to protect the implant's silicone coating. After at least one week of recovery, and prior to the first recording, the mouse was anesthetized and placed in a stereotaxic frame. The layer of durable silicone covering the SHIELD implant was removed. A ground wire was inserted into the grounding hole in the implant and pushed forward until it rested on the surface of the brain. A Duragel mixture was then prepared and poured over the implant to a thickness of at least 1 mm, then allowed to cure for at least 24 hours[84].

Recordings. To allow post-hoc identification of probe tracks, probes were coated with DS-DiD (2mM in ethanol; ThermoFisher Product #D12730) by immersing them in a well filled with dye. Each probe was dipped five times to ensure adequate coating. Each Neuropixels Opto probe was mounted on a 3-axis micromanipulator (New Scale Technologies, Victor, NY) on a custom modular insertion system. We used Pinpoint[85] to select the appropriate insertion coordinates and approach angle for the desired target structure. Probes were manually driven to the appropriate hole in the SHIELD implant and slowly lowered toward the surface of the brain. The operator observed real-time continuous electrophysiological signals to identify when the probe entered the brain. If the probe needed adjustment when attempting to insert (e.g. to avoid blood vessels), the probe was completely retracted out of the Duragel to prevent probe bending. If a probe could not be inserted into its assigned hole, another target hole was selected. Once all probes reached the brain surface, each probe was automatically inserted to its target depth at a speed of 200 μm/min. Once all probes reached their final depth, they were allowed to settle for 10 minutes, and photo documentation of the inserted probes was captured. Neuropixels data was acquired using the Open Ephys GUI[56] with gain settings of 500x and 250x for the AP and LFP bands. Videos of the eye, face, and/or body were acquired with USB3 cameras (Teledyne FLIR) and Bonsai software[86]. At the end of the recording session, probes were slowly retracted from the brain (~1 mm/min). To remove debris, probes were submerged in a 1% Tergazyme solution overnight then rinsed in deionized water the next day.

Optotagging. To identify recorded units reliably activated by light, we presented 20 Hz trains of 10 ms laser pulses with an average inter-trial interval of 300 ms. Blue light (450 or 473 nm) or red light (638 nm) was delivered via the PXI-mounted laser module or a two-channel laser combiner (Oxxius, France). Opto-tagged cells were identified by their significant increase in firing rate to at least 4 pulses from at least one emitter ($p < 0.05$, Holm-Sidak adjustment for multiple comparisons), a maximum spike latency of 8 ms, and a mean response reliability > 0.3.

Data processing. Neuropixels raw data files were compressed using WavPack[87] and transferred to an Amazon S3 bucket. We used a custom Nextflow pipeline running on the Code Ocean compute platform to run preprocessing, spike sorting, and curation. First, the data was decompressed and denoised using phase shift, high-pass filter, and median subtraction. Then, spike sorting was performed using Kilosort 2.5 [2]. Finally, we calculated a range of quality metrics (including inter-spike-interval violations ratio, amplitude cutoff, and presence ratio) for each unit. Each unit's location along the shank was estimated

based on the center of mass of the waveform amplitudes for recording sites within 75 µm of the peak. All functions are available in the SpikeInterface Python package[75].

Supplementary Figures

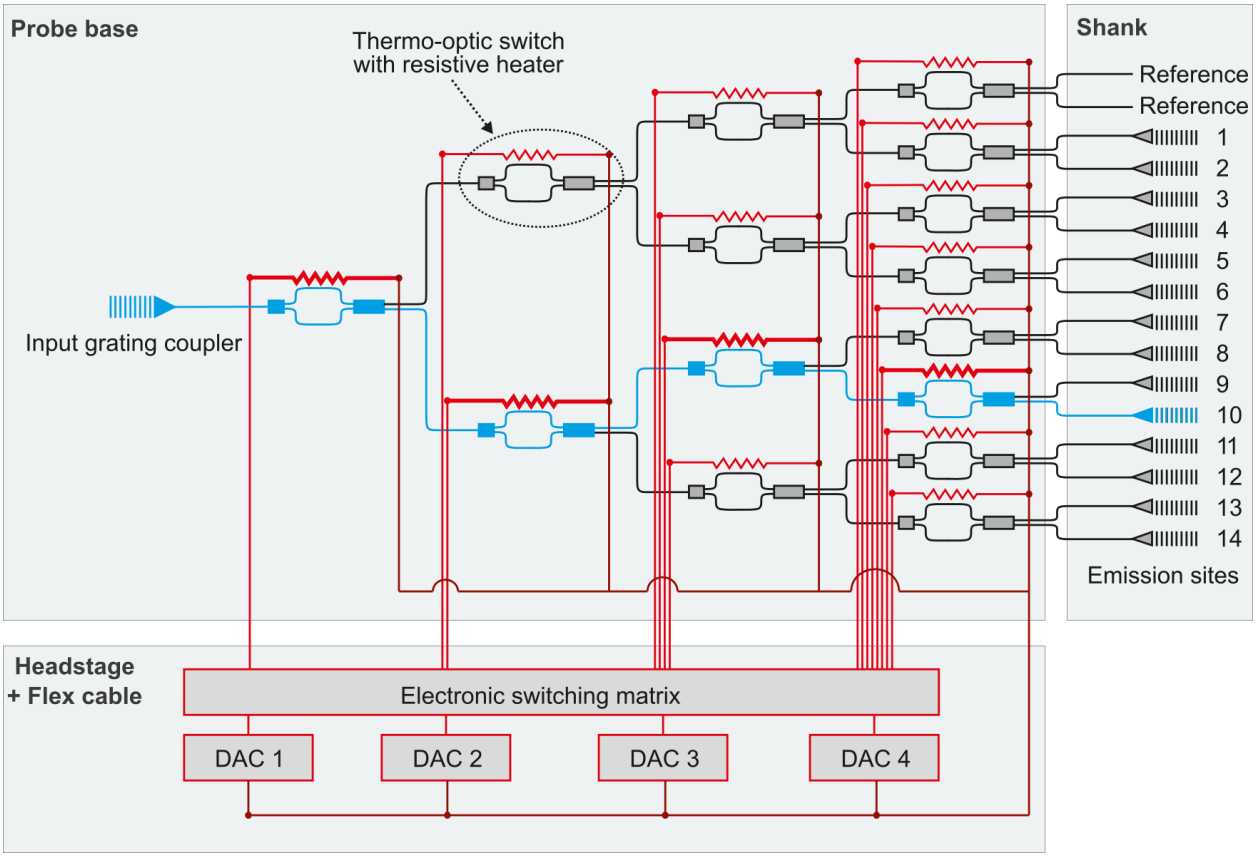

Figure S1 – Neuropixels Opto switching tree. Schematic of switching tree architecture, which distributes light from a single input grating coupler to one of fourteen waveguides on the shank. A network of 15 thermo-optic switches is controlled by four digital-to-analog converters (DACs), allowing light to be routed to each emitter, or to reference sites used for calibration. Each probe contains a separate switching tree for blue and red light.

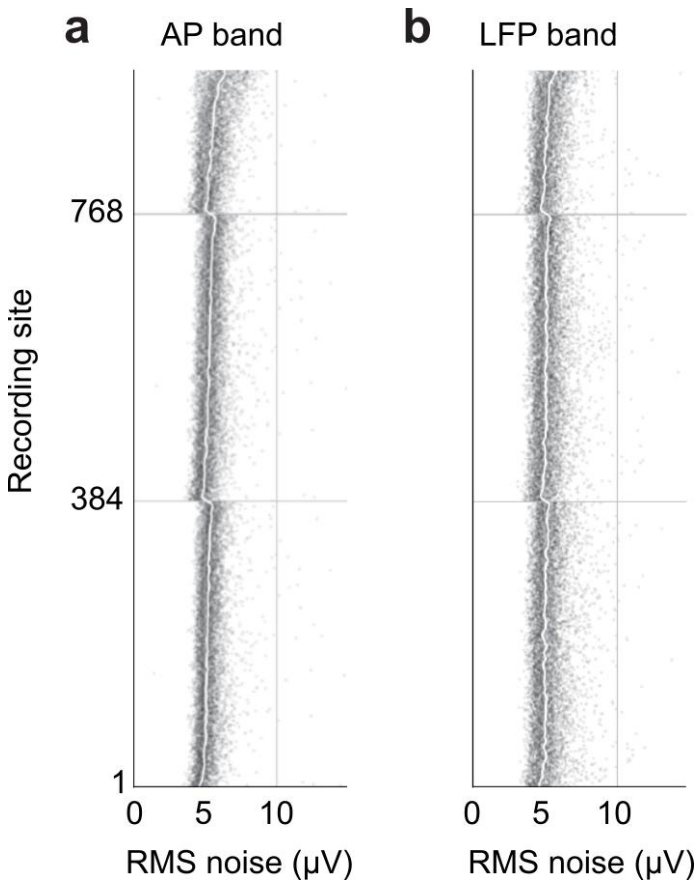

Figure S2 – Electrical characterization. a, Input-referred RMS noise levels, measured in saline for 960 recording sites from *N* = 21 probes, in the AP band. Each dot represents a measurement for one site for one probe. White line indicates the median across all probes. **b**, same, for the LFP band.

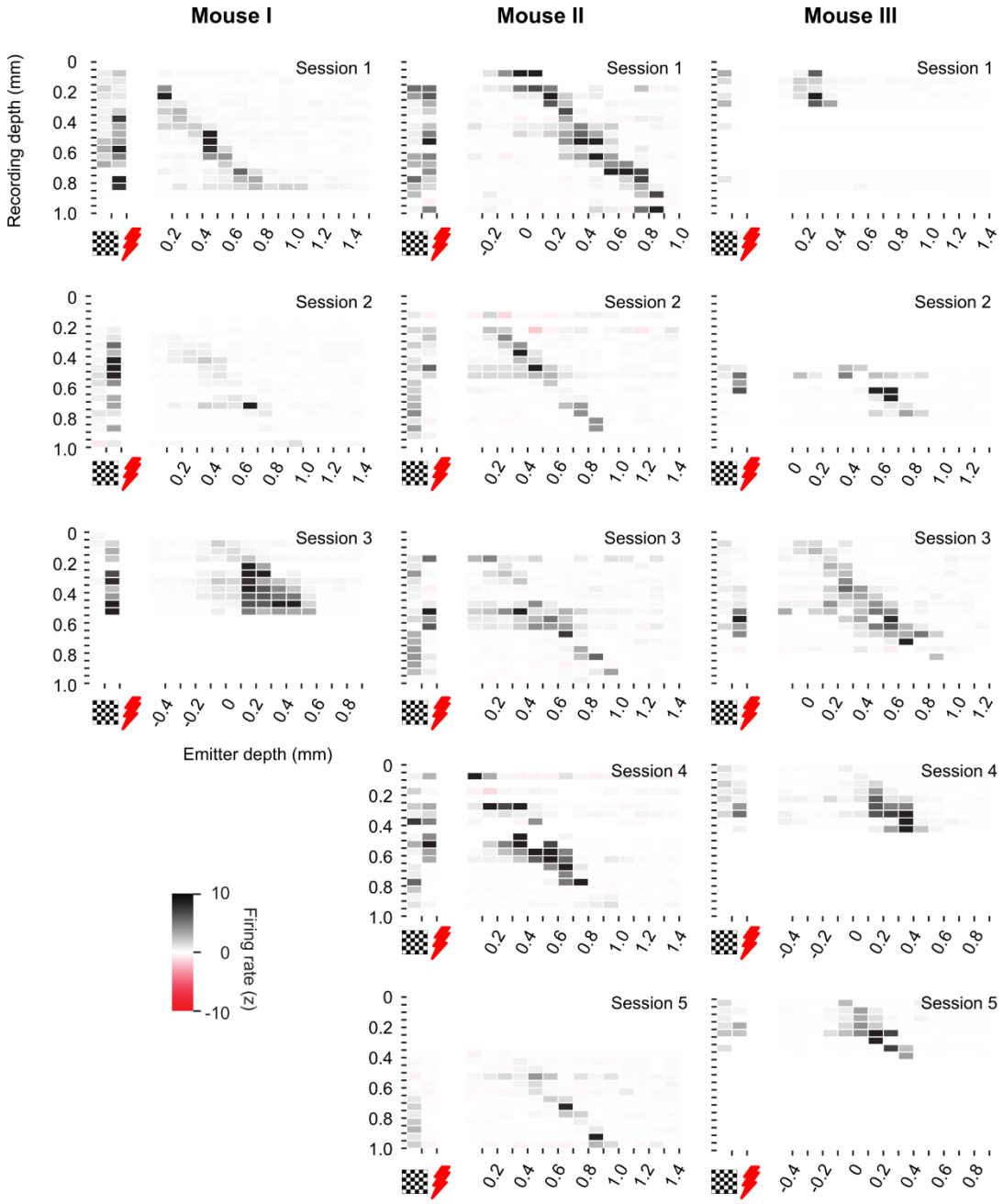

Figure S3 – Additional examples of local circuit activation. Results of all the sessions with the experiments shown in Figure 3. Format is as in Figure 3f, showing average over time of response during stimulation with visual stimulus, surface laser, and single emitters (abscissa), at different cortical depths (ordinate).

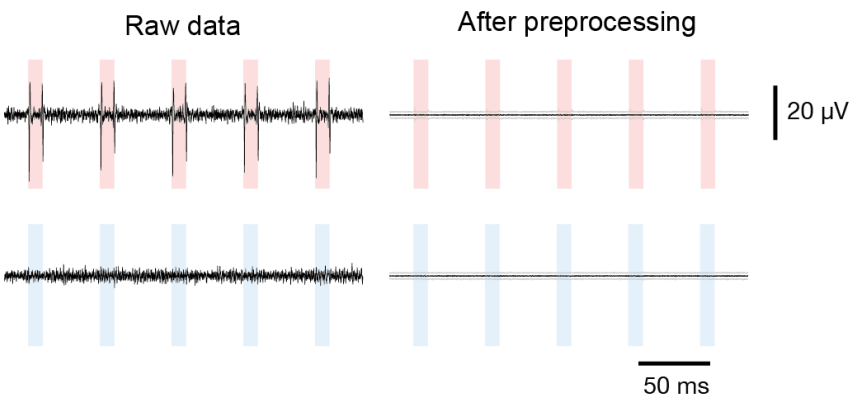

Figure S4 – Light artifact and removal. Light artifact for 10 ms red (top) and blue (bottom) light pulses at 100 μW, before and after standard pre-processing steps (average of 20 trials, 384 recording sites). The artifact seen for red pulses is highly uniform across recording sites, allowing it to be completely removed by phase shifting and median subtraction (see Methods for details).

Region	Cell type	Opsin	# Optotagged	Sessions	Mice
CP	D1 MSN	ChRmine	4	2	1
CP	D1 MSN	CoChR	150	17	10
CP	D2 MSN	ChRmine	3	3	1
CP	D2 MSN	BiPOLES	2	2	1
CP	D2 MSN	ChrimsonR	4	1	1
CP	D2 MSN	CoChR	99	12	7
CP	ChAT	ChRmine	5	2	2
CP	ChAT	BiPOLES	1	1	1
CP	ChAT	CoChR	3	1	1
GPe	Ntrk1	rsChRmine	3	1	1
MRN	Vglut2	ChRmine	17	1	1
MRN	Gad67	ChRmine	11	2	2

Supplementary Table 1 – Regions and cell types for subcortical optotagging. Details of optotagged units included in **Figure 5**. The number of units optotagged per session for a given cell type ranges between 1 and 28. Sessions may appear multiple times in this table as multiple cell types were tagged per session.

References

1 Jun, J. J. *et al.* Fully integrated silicon probes for high-density recording of neural activity. *Nature* **551**, 232-236 (2017). https://doi.org/10.1038/nature24636

2 Steinmetz, N. A. *et al.* Neuropixels 2.0: A miniaturized high-density probe for stable, long-term brain recordings. *Science* **372** (2021). https://doi.org/10.1126/science.abf4588

3 Cohen, J. Y., Haesler, S., Vong, L., Lowell, B. B. & Uchida, N. Neuron-type-specific signals for reward and punishment in the ventral tegmental area. *Nature* **482**, 85-88 (2012). https://doi.org/10.1038/nature10754

4 Li, N., Chen, T. W., Guo, Z. V., Gerfen, C. R. & Svoboda, K. A motor cortex circuit for motor planning and movement. *Nature* **519**, 51-56 (2015). https://doi.org/10.1038/nature14178

5 Lima, S. Q., Hromadka, T., Znamenskiy, P. & Zador, A. M. PINP: a new method of tagging neuronal populations for identification during in vivo electrophysiological recording. *PLoS One* **4**, e6099 (2009). https://doi.org/10.1371/journal.pone.0006099

6 Cardin, J. A. *et al.* Driving fast-spiking cells induces gamma rhythm and controls sensory responses. *Nature* **459**, 663-667 (2009). https://doi.org/10.1038/nature08002

7 Huber, D. *et al.* Sparse optical microstimulation in barrel cortex drives learned behaviour in freely moving mice. *Nature* **451**, 61-64 (2008). https://doi.org/10.1038/nature06445

8 Moreaux, L. C. *et al.* Integrated Neurophotonics: Toward Dense Volumetric Interrogation of Brain Circuit Activity-at Depth and in Real Time. *Neuron* **108**, 66-92 (2020). https://doi.org/10.1016/j.neuron.2020.09.043

9 Warden, M. R., Cardin, J. A. & Deisseroth, K. Optical neural interfaces. *Annu Rev Biomed Eng* **16**, 103-129 (2014). https://doi.org/10.1146/annurev-bioeng-071813-104733

10 Yizhar, O., Fenno, L. E., Davidson, T. J., Mogri, M. & Deisseroth, K. Optogenetics in neural systems. *Neuron* **71**, 9-34 (2011). https://doi.org/10.1016/j.neuron.2011.06.004

11 Buzsáki, G. *et al.* Tools for probing local circuits: high-density silicon probes combined with optogenetics. *Neuron* **86**, 92-105 (2015). https://doi.org/10.1016/j.neuron.2015.01.028

12 Kim, C. K., Adhikari, A. & Deisseroth, K. Integration of optogenetics with complementary methodologies in systems neuroscience. *Nat Rev Neurosci* **18**, 222-235 (2017). https://doi.org/10.1038/nrn.2017.15

13 Luo, L., Callaway, E. M. & Svoboda, K. Genetic Dissection of Neural Circuits: A Decade of Progress. *Neuron* **98**, 256-281 (2018). https://doi.org/10.1016/j.neuron.2018.03.040

14 Adesnik, H. & Naka, A. Cracking the Function of Layers in the Sensory Cortex. *Neuron* **100**, 1028-1043 (2018). https://doi.org/10.1016/j.neuron.2018.10.032

15 Gradinaru, V., Mogri, M., Thompson, K. R., Henderson, J. M. & Deisseroth, K. Optical deconstruction of parkinsonian neural circuitry. *Science* **324**, 354-359 (2009). https://doi.org/10.1126/science.1167093

16 Li, N. *et al.* Spatiotemporal constraints on optogenetic inactivation in cortical circuits. *eLife* **8** (2019). https://doi.org/10.7554/eLife.48622

17 Olsen, S. R., Bortone, D. S., Adesnik, H. & Scanziani, M. Gain control by layer six in cortical circuits of vision. *Nature* **483**, 47-52 (2012). https://doi.org/10.1038/nature10835

18 Economo, M. N. *et al.* Distinct descending motor cortex pathways and their roles in movement. *Nature* **563**, 79-84 (2018). https://doi.org/10.1038/s41586-018-0642-9

19 Lehtinen, K., Nokia, M. S. & Takala, H. Red Light Optogenetics in Neuroscience. *Front Cell Neurosci* **15**, 778900 (2021). https://doi.org/10.3389/fncel.2021.778900

20 Pisanello, F. *et al.* Dynamic illumination of spatially restricted or large brain volumes via a single tapered optical fiber. *Nat Neurosci* **20**, 1180-1188 (2017). https://doi.org/10.1038/nn.4591

21 Pisano, F. *et al.* Depth-resolved fiber photometry with a single tapered optical fiber implant. *Nat Methods* **16**, 1185-1192 (2019). https://doi.org/10.1038/s41592-019-0581-x

22 Stark, E., Koos, T. & Buzsaki, G. Diode probes for spatiotemporal optical control of multiple neurons in freely moving animals. *J Neurophysiol* **108**, 349-363 (2012). https://doi.org/10.1152/jn.00153.2012

23 Zorzos, A. N., Scholvin, J., Boyden, E. S. & Fonstad, C. G. Three-dimensional multiwaveguide probe array for light delivery to distributed brain circuits. *Opt Lett* **37**, 4841-4843 (2012). https://doi.org/10.1364/OL.37.004841

24 Ayub, S. *et al.* Compact Optical Neural Probes With Up to 20 Integrated Thin-Film muLEDs Applied in Acute Optogenetic Studies. *IEEE transactions on bio-medical engineering* **67**, 2603-2615 (2020). https://doi.org/10.1109/TBME.2020.2966293

25 Goßler, C. *et al.* GaN-based micro-LED arrays on flexible substrates for optical cochlear implants.

Journal of Physics D: Applied Physics **47** (2014). https://doi.org/10.1088/0022-3727/47/20/205401

26 Kim, T. I. *et al.* Injectable, cellular-scale optoelectronics with applications for wireless optogenetics. *Science* **340**, 211-216 (2013). https://doi.org/10.1126/science.1232437

27 Scharf, R. *et al.* Depth-specific optogenetic control in vivo with a scalable, high-density muLED neural probe. *Sci Rep* **6**, 28381 (2016). https://doi.org/10.1038/srep28381

28 Taal, A. J. *et al.* Optogenetic stimulation probes with single-neuron resolution based on organic LEDs monolithically integrated on CMOS. *Nature Electronics* **6**, 669-679 (2023). https://doi.org/10.1038/s41928-023-01013-y

29 Anikeeva, P. *et al.* Optetrode: a multichannel readout for optogenetic control in freely moving mice. *Nat Neurosci* **15**, 163-170 (2012). https://doi.org/10.1038/nn.2992

30 Chen, S. *et al.* A fiber-based implantable multi-optrode array with contiguous optical and electrical sites. *J Neural Eng* **10**, 046020 (2013). https://doi.org/10.1088/1741-2560/10/4/046020

31 Im, M., Cho, I. J., Wu, F., Wise, K. D. & Yoon, E. Neural Probes Integrated with Optical Mixer/Splitter Waveguides and Multiple Stimulation Sites. *Proc Ieee Micr Elect*, 1051-1054 (2011). https://doi.org/10.1109/MEMSYS.2011.5734609

32 Kim, E. G. *et al.* 3D silicon neural probe with integrated optical fibers for optogenetic modulation. *Lab Chip* **15**, 2939-2949 (2015). https://doi.org/10.1039/c4lc01472c

33 Royer, S. *et al.* Multi-array silicon probes with integrated optical fibers: light-assisted perturbation and recording of local neural circuits in the behaving animal. *Eur J Neurosci* **31**, 2279-2291 (2010). https://doi.org/10.1111/j.1460-9568.2010.07250.x

34 Ko, E., Vöröslakos, M., Buzsáki, G. & Yoon, E. Dual-color μ-LEDs integrated neural interface for multi-control optogenetic electrophysiology. *bioRxiv*, 2024.2007.2030.605927 (2024). https://doi.org/10.1101/2024.07.30.605927

35 Kwon, K. Y., Lee, H. M., Ghovanloo, M., Weber, A. & Li, W. Design, fabrication, and packaging of an integrated, wirelessly-powered optrode array for optogenetics application. *Front Syst Neurosci* **9**, 69 (2015). https://doi.org/10.3389/fnsys.2015.00069

36 Mao, D., Sun, F., Driscoll, B., Li, Z. & Xu, G. Close-packed dual-color micro-LEDs enable cortical-layer-specific bidirectional in vivo optogenetic electrophysiology. *Cell Reports Physical Science* **4** (2023). https://doi.org/10.1016/j.xcrp.2023.101702

37 Voroslakos, M. *et al.* HectoSTAR muLED Optoelectrodes for Large-Scale, High-Precision In Vivo Opto-Electrophysiology. *Adv Sci (Weinh)* **9**, e2105414 (2022). https://doi.org/10.1002/advs.202105414

38 Wu, F. *et al.* Monolithically Integrated muLEDs on Silicon Neural Probes for High-Resolution Optogenetic Studies in Behaving Animals. *Neuron* **88**, 1136-1148 (2015). https://doi.org/10.1016/j.neuron.2015.10.032

39 Christian, M. P., Smith, A. N. & Firebaugh, S. L. in *IEEE International Instrumentation and Measurement Technology Conference (I2mtc)*. 1420-1425.

40 Stujenske, J. M., Spellman, T. & Gordon, J. A. Modeling the Spatiotemporal Dynamics of Light and Heat Propagation for in vivo Optogenetics. *Cell Rep* **12**, 525-534 (2015). https://doi.org/10.1016/j.celrep.2015.06.036

41 Valero, M., Zutshi, I., Yoon, E. & Buzsaki, G. Probing subthreshold dynamics of hippocampal neurons by pulsed optogenetics. *Science* **375**, 570-574 (2022). https://doi.org/10.1126/science.abm1891

42 Kampasi, K. *et al.* Dual color optogenetic control of neural populations using low-noise, multishank optoelectrodes. *Microsyst Nanoeng* **4** (2018). https://doi.org/10.1038/s41378-018-0009-2

43 Lanzio, V. *et al.* Scalable nanophotonic neural probes for multicolor and on-demand light delivery in brain tissue. *Nanotechnology* **32** (2021). https://doi.org/10.1088/1361-6528/abef2a

44 Mohanty, A. *et al.* Reconfigurable nanophotonic silicon probes for sub-millisecond deep-brain optical stimulation. *Nat Biomed Eng* **4**, 223-231 (2020). https://doi.org/10.1038/s41551-020-0516-y

45 Roszko, D. A. *et al.* Foundry-fabricated dual-color nanophotonic neural probes for photostimulation and electrophysiological recording. *bioRxiv*, 2024.2009.2025.614961 (2024). https://doi.org/10.1101/2024.09.25.614961

46 Segev, E. *et al.* Patterned photostimulation via visible-wavelength photonic probes for deep brain optogenetics. *Neurophotonics* **4**, 011002 (2017). https://doi.org/10.1117/1.NPh.4.1.011002

47 Klapoetke, N. C. *et al.* Independent optical excitation of distinct neural populations. *Nat Methods* **11**, 338-346 (2014). https://doi.org/10.1038/nmeth.2836

48 Marshel, J. H. *et al.* Cortical layer-specific critical dynamics triggering perception. *Science* **365** (2019). https://doi.org/10.1126/science.aaw5202

49 Bosschaart, N., Edelman, G. J., Aalders, M. C., van Leeuwen, T. G. & Faber, D. J. A literature review and novel theoretical approach on the optical properties of whole blood. *Lasers Med Sci* **29**, 453-479 (2014). https://doi.org/10.1007/s10103-013-1446-7

50 Boyden, E. S., Zhang, F., Bamberg, E., Nagel, G. & Deisseroth, K. Millisecond-timescale, genetically targeted optical control of neural activity. *Nat Neurosci* **8**, 1263-1268 (2005). https://doi.org/10.1038/nn1525

51 Kerman, S. *et al.* Integrated Nanophotonic Excitation and Detection of Fluorescent Microparticles. *ACS Photonics* **4**, 1937-1944 (2017). https://doi.org/10.1021/acsphotonics.7b00171

52 Chen, X., Li, C., Fung, C. K. Y., Lo, S. M. G. & Tsang, H. K. Apodized Waveguide Grating Couplers for Efficient Coupling to Optical Fibers. *IEEE Photonics Technology Letters* **22**, 1156-1158 (2010). https://doi.org/10.1109/lpt.2010.2051220

53 Sacher, W. D. *et al.* Implantable photonic neural probes for light-sheet fluorescence brain imaging. *Neurophotonics* **8** (2021). https://doi.org/10.1117/1.NPh.8.2.025003

54 Neutens, P. *et al.* in *2023 International Electron Devices Meeting (IEDM)* (IEEE, San Francisco, CA, USA, 2023).

55 Liu, S. *et al.* Thermo-optic phase shifters based on silicon-on-insulator platform: state-of-the-art and a review. *Front Optoelectron* **15**, 9 (2022). https://doi.org/10.1007/s12200-022-00012-9

56 Siegle, J. H. *et al.* Open Ephys: an open-source, plugin-based platform for multichannel electrophysiology. *J Neural Eng* **14**, 045003 (2017). https://doi.org/10.1088/1741-2552/aa5eea

57 Zhang, F., Wang, L. P., Boyden, E. S. & Deisseroth, K. Channelrhodopsin-2 and optical control of excitable cells. *Nat Methods* **3**, 785-792 (2006). https://doi.org/10.1038/nmeth936

58 Aravanis, A. M. *et al.* An optical neural interface: in vivo control of rodent motor cortex with integrated fiberoptic and optogenetic technology. *J Neural Eng* **4**, S143-156 (2007). https://doi.org/10.1088/1741-2560/4/3/S02

59 Harris, K. D., Henze, D. A., Csicsvari, J., Hirase, H. & Buzsaki, G. Accuracy of tetrode spike separation as determined by simultaneous intracellular and extracellular measurements. *J Neurophysiol* **84**, 401-414 (2000). https://doi.org/10.1152/jn.2000.84.1.401

60 Henze, D. A. *et al.* Intracellular features predicted by extracellular recordings in the hippocampus in vivo. *J Neurophysiol* **84**, 390-400 (2000). https://doi.org/10.1152/jn.2000.84.1.390

61 Chan, K. Y. *et al.* Engineered AAVs for efficient noninvasive gene delivery to the central and peripheral nervous systems. *Nat Neurosci* **20**, 1172-1179 (2017). https://doi.org/10.1038/nn.4593

62 Guo, Z. V. *et al.* Flow of cortical activity underlying a tactile decision in mice. *Neuron* **81**, 179-194 (2014). https://doi.org/10.1016/j.neuron.2013.10.020

63 Bartho, P. *et al.* Characterization of neocortical principal cells and interneurons by network interactions and extracellular features. *J Neurophysiol* **92**, 600-608 (2004). https://doi.org/10.1152/jn.01170.2003

64 Toyama, K., Kimura, M. & Tanaka, K. Organization of cat visual cortex as investigated by cross-correlation technique. *J Neurophysiol* **46**, 202-214 (1981). https://doi.org/10.1152/jn.1981.46.2.202

65 Hunker, A. C. *et al.* Enhancer AAV toolbox for accessing and perturbing striatal cell types and circuits. *bioRxiv*, 2024.2009.2027.615553 (2024). https://doi.org/10.1101/2024.09.27.615553

66 Kishi, K. E. *et al.* Structural basis for channel conduction in the pump-like channelrhodopsin ChRmine. *Cell* **185**, 672-689 e623 (2022). https://doi.org/10.1016/j.cell.2022.01.007

67 Vierock, J. *et al.* BiPOLES is an optogenetic tool developed for bidirectional dual-color control of neurons. *Nat Commun* **12**, 4527 (2021). https://doi.org/10.1038/s41467-021-24759-5

68 Madisen, L. *et al.* A toolbox of Cre-dependent optogenetic transgenic mice for light-induced activation and silencing. *Nat Neurosci* (2012). https://doi.org/10.1038/nn.3078

69 Hippenmeyer, S. *et al.* A developmental switch in the response of DRG neurons to ETS transcription factor signaling. *PLoS Biol* **3**, e159 (2005). https://doi.org/10.1371/journal.pbio.0030159

70 International Brain Laboratory *et al.* Standardized and reproducible measurement of decision-making in mice. *eLife* **10** (2021). https://doi.org/10.7554/eLife.63711

71 Goldey, G. J. *et al.* Removable cranial windows for long-term imaging in awake mice. *Nat Protoc* **9**, 2515-2538 (2014). https://doi.org/10.1038/nprot.2014.165

72 Jackson, N. & Muthuswamy, J. Artificial dural sealant that allows multiple penetrations of implantable brain probes. *J Neurosci Methods* **171**, 147-152 (2008). https://doi.org/10.1016/j.jneumeth.2008.02.018

73 Ragan, T. *et al*. Serial two-photon tomography for automated ex vivo mouse brain imaging. *Nat Methods* **9**, 255-258 (2012). https://doi.org/10.1038/nmeth.1854

74 Matveev, P. *et al*. Simultaneous mesoscopic measurement and manipulation of mouse cortical activity. *bioRxiv*, 2024.2011.2001.621418 (2024). https://doi.org/10.1101/2024.11.01.621418

75 Buccino, A. P. *et al*. SpikeInterface, a unified framework for spike sorting. *eLife* **9** (2020). https://doi.org/10.7554/eLife.61834

76 Pachitariu, M., Sridhar, S., Pennington, J. & Stringer, C. Spike sorting with Kilosort4. *Nat Methods* **21**, 914-921 (2024). https://doi.org/10.1038/s41592-024-02232-7

77 Beau, M., D'Agostino, F., Lajko, A., Martínez, G. & Kostadinov, D. in *Zenodo* https://doi.org/10.5281/zenodo.5509733 (2021).

78 Rossi, J. *et al*. Melanocortin-4 receptors expressed by cholinergic neurons regulate energy balance and glucose homeostasis. *Cell Metab* **13**, 195-204 (2011). https://doi.org/10.1016/j.cmet.2011.01.010

79 Zhang, J. *et al*. c-Fos facilitates the acquisition and extinction of cocaine-induced persistent changes. *J Neurosci* **26**, 13287-13296 (2006). https://doi.org/10.1523/JNEUROSCI.3795-06.2006

80 Vong, L. *et al*. Leptin action on GABAergic neurons prevents obesity and reduces inhibitory tone to POMC neurons. *Neuron* **71**, 142-154 (2011). https://doi.org/10.1016/j.neuron.2011.05.028

81 Hwang, H. W. *et al*. cTag-PAPERCLIP Reveals Alternative Polyadenylation Promotes Cell-Type Specific Protein Diversity and Shifts Araf Isoforms with Microglia Activation. *Neuron* **95**, 1334-1349 e1335 (2017). https://doi.org/10.1016/j.neuron.2017.08.024

82 Groblewski, P. A. *et al*. A standardized head-fixation system for performing large-scale, in vivo physiological recordings in mice. *J Neurosci Methods* **346**, 108922 (2020). https://doi.org/10.1016/j.jneumeth.2020.108922

83 Bennett, C. *et al*. SHIELD: Skull-shaped hemispheric implants enabling large-scale electrophysiology datasets in the mouse brain. *Neuron* **112**, 2869-2885 e2868 (2024). https://doi.org/10.1016/j.neuron.2024.06.015

84 Lakunina, A. in *protocols.io* (2024).

85 Birman, D. *et al*. Pinpoint: trajectory planning for multi-probe electrophysiology and injections in an interactive web-based 3D environment. *bioRxiv*, 2023.2007.2014.548952 (2023). https://doi.org/10.1101/2023.07.14.548952

86 Lopes, G. *et al*. Bonsai: an event-based framework for processing and controlling data streams. *Front Neuroinform* **9**, 7 (2015). https://doi.org/10.3389/fninf.2015.00007

87 Buccino, A. P. *et al*. Compression strategies for large-scale electrophysiology data. *J Neural Eng* **20** (2023). https://doi.org/10.1088/1741-2552/acf5a4